Broadband Differentially Fed Tapered Slot Antenna Array for Radio Astronomy Applications

Michel Arts [#1], Rob Maaskant [#2], Eloy de Lera Acedo [*3], Jan Geralt bij de Vaate [#4]

[#] *Netherlands Institute for Radio Astronomy (ASTRON)*
P.O. Box 2, 7990 AA Dwingeloo, the Netherlands
[1] arts@astron.nl
[2] maaskant@astron.nl
[4] vaate@astron.nl

[*] *University of Cambridge*
Rutherford Building, Cavendish Laboratory, JJ Thomson Avenue, Cambridge CB3 0HE, United Kingdom
[3] eloy@mrao.cam.ac.uk

***Abstract*— This paper describes the preliminary design results of a differentially fed tapered slot antenna. Traditional unbalanced tapered slot antennas often employ a bilateral strip line feed, or a separate feed board, in combination with a potentially lossy radial stub and microstrip line (balun). In order to reduce the associated transmission line losses, a differentially fed tapered slot antenna is considered. Main focus is on the measurement procedure and the determination of the active reflection coefficient. The properties of the (undesired) common modes are also discussed. Finally, the effective area for broadside is determined and turned out to be larger than 80% of the physical aperture area of the array.**

I. Introduction

The international radio-astronomical community is currently developing plans for a radio telescope with an effective area of one square kilometer, known as the Square Kilometer Array (SKA). The European SKA concept considers the use of aperture phased-array antennas [1]. As a part of the European feasibility study, the Netherlands Institute for Radio Astronomy (ASTRON) is investigating the possibilities to reduce the material and production costs of phased array antennas, in particular of dual-polarized arrays of tapered slot antennas [2]. In fact, a demonstrator array of low-cost elements with a specified aperture area of 400 m^2 (EMBRACE) is currently being built [3].

A major disadvantage of conventional (stripline-fed) tapered slot antenna arrays is that a separate feeding structure/balun is required, typically composed of a radial stub and a transmission line, which is potentially lossy. Because one is aiming for a system noise temperature of 50K, these losses can have a significant contribution to the system noise temperature (0.1 dB loss increases the system noise temperature by $\sim$ 7K). To overcome this drawback, a differentially fed tapered slot antenna array, which is conceptually based upon [4], has been examined in parallel with the development of EMBRACE. Another advantage of a differentially fed tapered slot antenna is that the production costs can be reduced. This paper describes the design of such an antenna array for a frequency band ranging from 300–1000 MHz.

We point out that the differential antenna outputs require an interface to differential receiver technology. For this purpose, separate (design) studies are ongoing with the objective to achieve an optimal low-noise low-cost differential amplifier design [5].

The construction of the array is described in II. The measurement method is described in Section III. The active reflection coefficient for both common and differential mode is discussed in Section IV. The measurements are compared to simulations in Section V. The effective area is discussed in Section VI and the conclusions are drawn in Section VII.

II. Description of the Array

Figure 1 illustrates a part of the interior of the array structure during its construction phase. The antenna elements are screen printed on a foil using silver ink and have been copper plated afterwards. The advantage of the differential structure is that both the feed line and antenna can be printed on the same layer, which simplifies and reduces the cost of the fabrication process. The attached PCBs contain both the bonding between the groundplanes of the coupled coplanar wave guide on the foil as well as the LNAs (in the final array design). One can observe

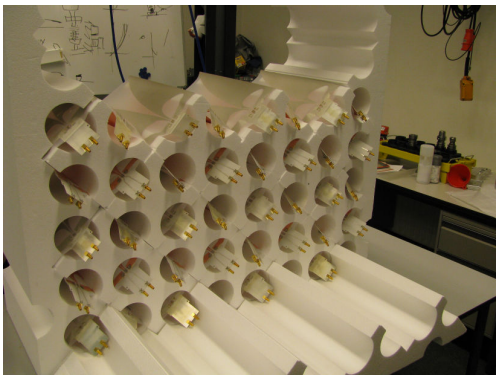

Fig. 1. The interior of the dual polarized Vivaldi array.

the manner in which the foil with printed antenna elements has been folded and placed into the foam supporting structure. It

has been conjectured that, even though the absorption losses of the foam are expected to be low, the cylindrical holes inside the supporting structure may further reduce the foam losses as well as the associated noise contribution. Figure 2 shows a detailed view of the foil. In the final fully phase-steered array, each of

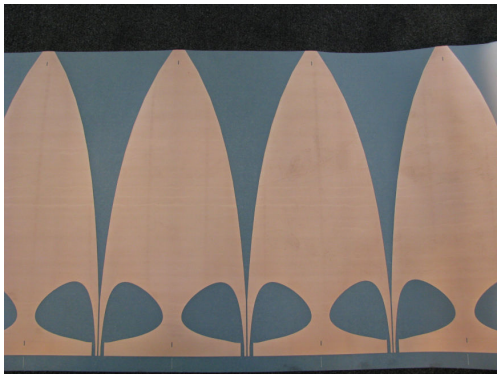

Fig. 2. Part of the foil with antenna elements.

the antenna elements will be connected to a differential Low Noise Amplifier (LNA), providing a low noise figure while achieving a large Common Mode Rejection Ratio (CMRR). The CMRR improves the second order intermodulation, which is important for wide-band array systems.

III. Measurement Procedure

To be able to measure the common mode properties of the array each element is equipped with two (asymmetric) single-ended ports instead of a differential (symmetrical) one. These single-ended ports have SMA-connectors. Using a four-port network analyzer the whole S-parameter set of the array is measured. Because the array is symmetric, the number of S-parameters that have to be measured can be reduced.

The S-matrix is measured including the feed boards between each antenna element and its two SMA-connectors. After the measurements the reference point has to be shifted from the SMA-connectors to the point where each antenna element is connected to its feed board by compensating for the transmission-line length. For this purpose, we assumed a low insertion loss and return loss of the feed boards. After shifting the reference point, the reference impedance has been renormalized from 50 to 75 Ω. This is done because the antenna is designed for a reference impedance of 150 Ω (note that the S-matrix is the matrix with the couplings between the single-ended ports, a characteristic impedance of 150 Ω for a differential port corresponds with a characteristic impedance of 75 Ω of the single-ended ports).

From the renormalized S-matrix of the single-ended ports, the differential and common mode properties of the array can be derived. One symmetric port consists of two asymmetric single-ended ports p and q. The incident waves on the two single-ended ports of port n are denoted by $a_{p,n}$ and $a_{q,n}$. The corresponding reflected waves are denoted by $b_{p,n}$ and $b_{q,n}$. If port n is excited by a differential mode $a_{diff,n} = 1$ the excitation of the single-ended ports is $a_{p,n} = 1$ and $a_{q,n} = -1$. If port n is excited by a common mode $a_{comm,n} = 1$ the excitation of the single-ended ports is $a_{p,n} = 1$ and $a_{q,n} = 1$. In general, for a linear combination of common mode wave amplitude $a_{comm,n}$ and a differential mode wave amplitude $a_{diff,n}$ the incoming waves of the single-ended ports $a_{p,n}$ and $a_{q,n}$ are given by

$$\begin{aligned} a_{p,n} &= a_{comm,n} + a_{diff,n} \\ a_{q,n} &= a_{comm,n} - a_{diff,n} \end{aligned} \tag{1}$$

The differential and common mode as a function of the incoming waves of the sub ports p and q can be obtained by the inverse of (1):

$$\begin{aligned} a_{diff,n} &= \frac{1}{2}a_{p,n} - \frac{1}{2}a_{q,n} \\ a_{comm,n} &= \frac{1}{2}a_{p,n} + \frac{1}{2}a_{q,n} \end{aligned} \tag{2}$$

For the reflected waves $b_{p,m}$, $b_{q,m}$, $b_{diff,m}$ and $b_{comm,m}$ a similar relation can be derived. As an example, the differential and common mode of a reflected wave can be derived from the reflected waves from the sub ports p and q by (we will use this relation later on):

$$\begin{aligned} b_{diff,m} &= \frac{1}{2}b_{p,m} - \frac{1}{2}b_{q,m} \\ b_{comm,m} &= \frac{1}{2}b_{p,m} + \frac{1}{2}b_{q,m} \end{aligned} \tag{3}$$

The coupling between the single-ended ports of element m and n is given as

$$\begin{aligned} b_{p,m} &= S_{pp,mn}a_{p,n} + S_{pq,mn}a_{q,n} \\ b_{q,m} &= S_{qp,mn}a_{p,n} + S_{qq,mn}a_{q,n} \end{aligned} \tag{4}$$

By substituting (1) into (4), (4) into (3) and writing the results in matrix notation we get

$$\begin{pmatrix} \mathbf{b}_{diff} \\ \mathbf{b}_{comm} \end{pmatrix} = \begin{pmatrix} \mathbf{S}_{diffdiff} & \mathbf{S}_{diffcomm} \\ \mathbf{S}_{commdiff} & \mathbf{S}_{commcomm} \end{pmatrix} \begin{pmatrix} \mathbf{a}_{diff} \\ \mathbf{a}_{comm} \end{pmatrix} \tag{5}$$

The elements m, n of the sub matrices $\mathbf{S}_{diffdiff}$, $\mathbf{S}_{diffcomm}$, $\mathbf{S}_{commdiff}$ and $\mathbf{S}_{commcomm}$ are defined by

$$\begin{aligned} S_{diffdiff,mn} &= \frac{S_{pp,mn} - S_{pq,mn} - S_{qp,mn} + S_{qq.mn}}{2} \\ S_{diffcomm,mn} &= \frac{S_{pp,mn} + S_{pq,mn} - S_{qp,mn} - S_{qq.mn}}{2} \\ S_{commdiff,mn} &= \frac{S_{pp,mn} - S_{pq,mn} + S_{qp,mn} - S_{qq.mn}}{2} \\ S_{commcomm,mn} &= \frac{S_{pp,mn} + S_{pq,mn} + S_{qp,mn} + S_{qq.mn}}{2} \end{aligned} \tag{6}$$

The vectors $\mathbf{a}_{diff}$, $\mathbf{a}_{comm}$, $\mathbf{b}_{diff}$ and $\mathbf{b}_{comm}$ are defined by

$$\begin{aligned} \mathbf{a}_{diff} &= (a_{diff,1} \dots a_{diff,n} \dots a_{diff,N})^T \\ \mathbf{a}_{comm} &= (a_{comm,1} \dots a_{comm,n} \dots a_{comm,N})^T \\ \mathbf{b}_{diff} &= (b_{diff,1} \dots b_{diff,n} \dots b_{diff,N})^T \\ \mathbf{b}_{comm} &= (b_{comm,1} \dots b_{comm,n} \dots b_{comm,N})^T \end{aligned} \tag{7}$$

where N is the number of elements and T denotes the matrix transpose.

IV. Active Reflection Coefficient for Broadside

In general the active reflection coefficient of element m for a scan direction (θ_0, φ_0) is calculated as

$$\begin{aligned}\Gamma_{act,m}(\theta_0,\varphi_0) &= \sum_{n=1}^{N} S_{mn} e^{-jk(x_n \sin\theta_0 \cos\varphi_0 + y_n \sin\theta_0 \sin\varphi_0)} \\ &= \sum_{n=1}^{N} S_{mn} e^{-jk(x_n u + y_n v)}\end{aligned} \tag{8}$$

with

$$\begin{aligned}u &= \sin\theta_0 \cos\varphi_0 \\ v &= \sin\theta_0 \sin\varphi_0\end{aligned} \tag{9}$$

where (x_n, y_n) is the position of element n, k the wavenumber and N the number of elements. Because the sine and cosine functions are always between -1 and 1 for real-valued angles the following relation between u and v holds:

$$u^2 + v^2 \leq 1 \tag{10}$$

The region in the u, v-plane for which this relation holds is called the "visible space".

Each of the four sub matrices mentioned in Section III can be used to calculate four different active reflection coefficients. Figure 3 shows the active reflection coefficient for broadside ($u = 0$, $v = 0$) of one of the four center elements calculated by using the $\mathbf{S}_{diffdiff}$ matrix. We will refer to this reflection coefficient as the differential mode active reflection coefficient. The differential mode active reflection coefficient

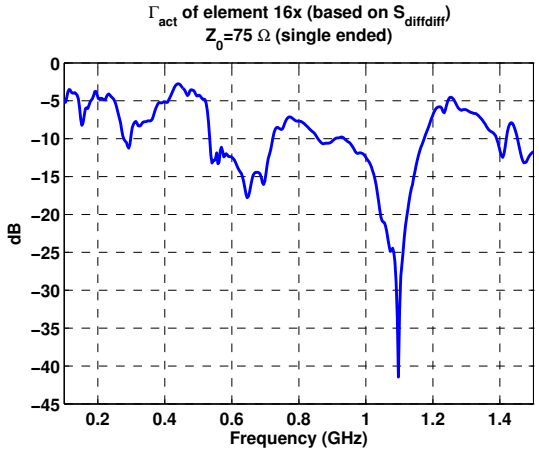

Fig. 3. Differential mode active reflection coefficient of one of the four center elements at broadside.

shows the amount of differential mode power that is reflected if all elements are excited differentially. Figure 4 shows the same for all x-polarized elements. One can see that the differential mode active reflection coefficient is below -5 dB between 0.6 and 1.2 GHz. This is not very good compared to the specification of -10 dB. The active reflection coefficient for broadside of all x-polarized elements calculated by using the

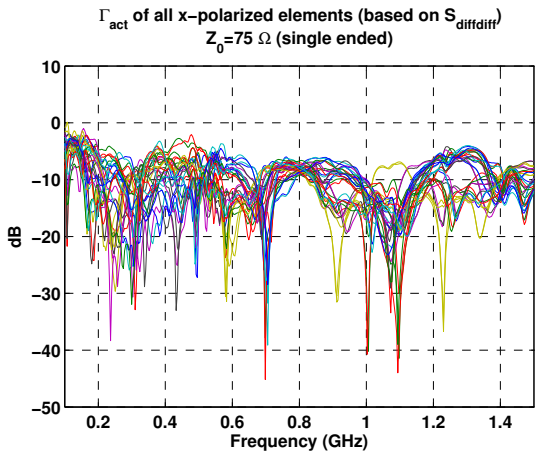

Fig. 4. Differential mode active reflection coefficient of all x-polarized elements at broadside.

$\mathbf{S}_{commcomm}$ matrix is shown in figure 5. We will call this active reflection coefficient the common mode active reflection coefficient. The active reflection coefficient is near 0 dB for

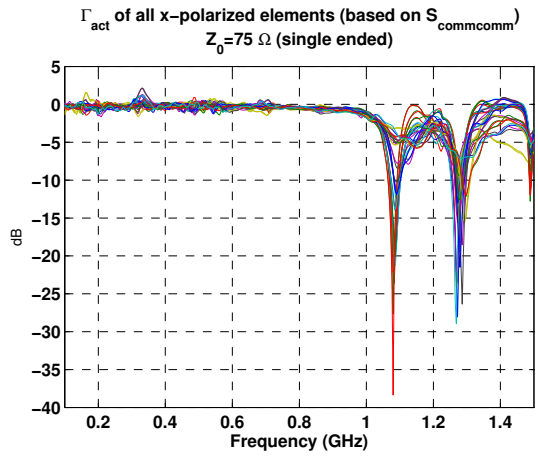

Fig. 5. Common mode active reflection coefficient of all x-polarized elements at broadside.

most frequencies. This means that if the antenna is excited with a common mode signal all common mode power will be reflected. I.e. a common mode signal will not be radiated by the array. This can be explained by the fact that the antenna elements act in 'monopole'-mode if they are excited with a common mode signal. The field of this mode will not be radiated but contributes to the surface wave of the array. Note that the active reflection can be larger than 0 dB for some elements. Because the active reflection coefficient for other elements is less than 0 dB this does not violate the law of conservation of energy. Figure 6 shows the active reflection coefficient for broadside of all x-polarized elements by using the $\mathbf{S}_{commdiff}$ matrix. This active reflection coefficient is a measure of the cross talk between the incident differential mode and the reflected common mode. It is below -10 dB for all frequencies and even below -20 dB between approximately

0.2 and 1 GHz. Ideally an incident differential mode should not cause a reflected common mode.

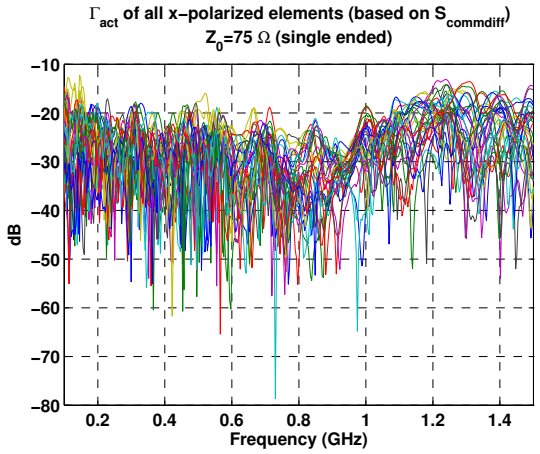

Fig. 6. Active reflection coefficient (based on $S_{commdiff}$) of all x-polarized elements at broadside.

V. Comparison with Simulations

The array has been designed using an infinite array approach. After the S-parameters of the array were measured, a finite array simulation was performed to verify the results. However, the array is too large to perform a full S-parameter simulation with single-ended ports in the frequency domain. For that reason, the two single-ended ports of each element were replaced by a single differential port and the array was simulated in the time-domain for one excitation. Figure 7 shows the simulated differential mode active reflection coefficient of the infinite and finite array simulations together with the measured differential mode active reflection coefficient. The differential mode active reflection coefficient of the finite

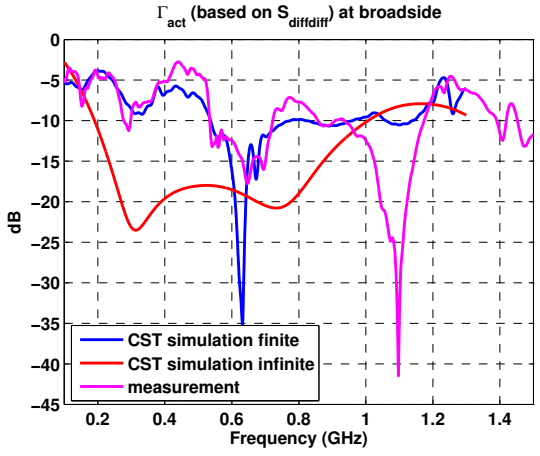

Fig. 7. Simulated differential mode active reflection coefficient of both a finite and an infinite array. The measured differential mode active reflection coefficient is shown as well.

array simulation and measurement is determined at one of the four center elements. One can see that the infinite array simulation predicts an active reflection coefficient of less than -10 dB between 0.2 and 1 GHz. The finite array simulation is rather different from the infinite array simulation which shows that the finite array effects are significant. As expected, the measurements are much closer to the finite array simulations.

Because a full S-parameter simulation could not be performed, the common mode active reflection coefficient could not be computed. It is however possible to perform a simulation in which all single-ended ports of all x-polarized elements are excited. Figure 8 shows the finite array simulation of the single-ended active reflection coefficient for all elements (all single-ended ports are excited by the same amplitude and phase). For this calculation the characteristic impedance of

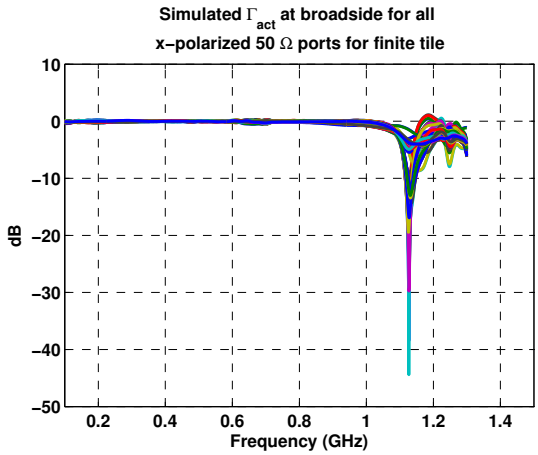

Fig. 8. Simulated single-ended active reflection coefficients for all x-polarized elements.

each single-ended port has not been renormalized to 75 Ω (so $Z_0 = 50\Omega$).

The simulated and measured single-ended active reflection coefficient of element 16x (center element) is shown in figure 9 One can see that this measured and simulated single-ended

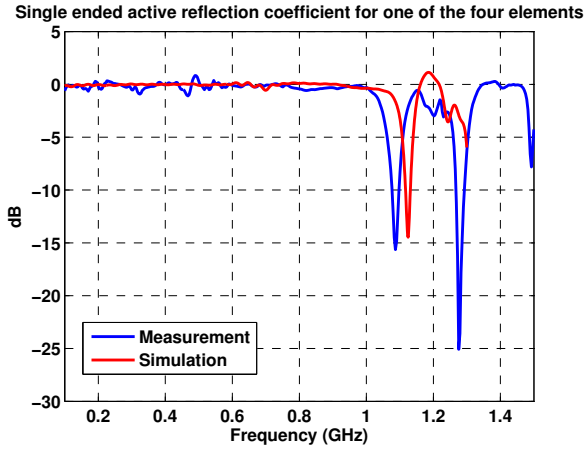

Fig. 9. Measured and simulated single-ended active reflection coefficient of one of the four center elements.

active reflection coefficient are in good agreement.

VI. Receiving Cross Section

In general, the receiving cross section of an element in an infinite array can be determined by [6]

$$A_r(\theta,\varphi) = \eta A_{ph}(1-|\Gamma_{act}(\theta,\varphi)|^2)\cos\theta \qquad (11)$$

with A_{ph} the physical area of one unit cell, θ the scan angle and η the antenna efficiency. The term η is not commonly used but can be easily derived by using equation (33) of [6]. The efficiency η is defined as

$$\eta = \frac{P_{tr}}{P_{acc}} \qquad (12)$$

with P_{tr} the transmitted power and P_{acc} the accepted power of the antenna.

We define the differential mode antenna efficiency η_{diff} as

$$\begin{aligned}\eta_{diff} &= \frac{P_{tr}}{P_{acc}} = \frac{|a_{diff}|^2-|b_{diff}|^2-|b_{comm}|^2}{|a_{diff}|^2-|b_{diff}|^2} \\ &= \frac{1-|\Gamma_{act,diff}(\theta,\varphi)|^2-|S^{act}_{comm,diff}(\theta,\varphi)|^2}{1-|\Gamma_{act,diff}(\theta,\varphi)|^2}\end{aligned} \qquad (13)$$

with $\Gamma_{act,diff}(\theta,\varphi)$ the differential mode active reflection coefficient and $S^{act}_{comm,diff}(\theta,\varphi)$ the coupling between the common and differential mode for an antenna element in a unit cell. Combining (11) and (13) gives for the differential receiving cross section

$$A_{r,diff}(\theta,\varphi) = A_{ph}(1-|\Gamma_{act,diff}(\theta,\varphi)|^2-|S^{act}_{comm,diff}(\theta,\varphi)|^2)\cos\theta \qquad (14)$$

The differential receiving cross section is the ratio between the received differential mode power and the power flux density of an incoming plane wave from direction (θ,φ). It is assumed that the polarization of the plane wave matches with the polarization of the antenna for that direction.

Figure 10 exemplifies the ratio between the differential receiving cross section $A_{r,diff}$ and the physical area A_{ph} of a unit cell for broadside as a function of frequency. One can observe that this ratio is larger than -1 dB (80%) over the largest part of the frequency band, which ranges from 0.3 to 1.0 GHz.

VII. Conclusions

The difference between the simulated (infinite array) and measured (finite array) active reflection coefficient is significant. The finite array simulation showed a better agreement implying that the finite array effects are significant. The common mode active reflection coefficient for broadside is almost 0 dB for most part of the frequency band. This means that the receiving cross section for the common mode is approximately zero for broadside. The receiving cross section for the differential mode is more than 80% of the physical area for the largest part of the frequency band.

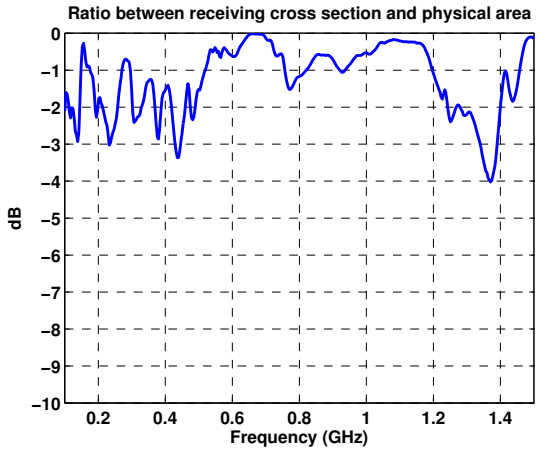

Fig. 10. Ratio $A_{r,diff}/A_{ph}$ of one of the center elements for broadside as a function of frequency.

Acknowledgements

This work has been supported by NL-IS-PACMAN and EU-FP6 SKADS. The antenna foil production has been sponsored by MECO Equipment Engineers B.V.

References

[1] Website: *http://www.skads-eu.org*

[2] R. Maaskant, M. Popova, and R. van de Brink, "Towards the Design of a Low Cost Wideband Demonstrator Tile for the SKA," Proc. European Conf. on Antennas and Propag., Nice, France, 2006.

[3] P.D. Patel, G.W. Kant, E. van de Wal, and A. van Ardenne, "Towards Completion of Aperture Array Developments – EMBRACE Update," URSI-General Assembly, Chicago, Aug. 2008.

[4] R. Maaskant, "Antenne-Inrichting, Antenne-Array, Samenstel voor het Assembleren van een Antenne-Array en een Elektronische Inrichting Omvattende een Antenne," Dutch patent, no. NL1034102.

[5] J.G. bij de Vaate, L. Bakker, E. E. M. Woestenburg, R. H. Witvers, G. W. Kant, W. van Capellen, "Low Cost Low Noise Phased-Array Feeding Systems for SKA Pathfinders," accepted for the ANTEM2009 conference, Banff, Canada, Feb. 2009.

[6] C. Craeye and M. Arts, "On the Receiving Cross Section of an Antenna in Infinite Linear and Planar Arrays," Radio Science, Vol. 39, Apr. 2004, pp. 1–8.